A Comparison of Three Different Modeling Strategies for Evaluating Cloud and Radiation Parameterizations

STEVEN J. GHAN AND L. RUBY LEUNG

Atmospheric Sciences Group, Pacific Northwest National Laboratory, Richland, Washington

JAMES MCCAA

Department of Atmospheric Sciences, University of Washington, Seattle, Washington

(Manuscript received 24 April 1998, in final form 20 October 1998)

ABSTRACT

Parallel simulations of clouds and radiation fields by a single-column model (SCM), a regional circulation model, and a global circulation model (GCM), each using the same treatment of all physical processes and approximately the same spatial resolution, are compared with observations at the Atmopheric Radiation Measurement Clouds and Radiation Testbed in the southern Great Plains. Significant differences between model simulations are evident for individual cloud systems, but these differences are not systematic, varying from cloud system to cloud system. Several systematic differences between model simulations and observations are identified. These biases are about the same for each model and are much larger than differences between model simulations, suggesting that for some purposes one model can serve as a testbed for parameterizations developed for another.

The role of nudging in the simulations is explored by driving the SCM with large-scale forcing from a GCM simulation. The authors find that nudging of SCM temperature and humidity toward the GCM simulation, using the inverse of the advective timescale for the nudging coefficient, reduces errors in the SCM simulation when artificial errors in the forcing are introduced. The authors also find that nudging of temperature and humidity hides physics errors introduced in the SCM, but only if the physics errors involve processes that directly influence temperature or humidity. Thus, errors in the treatment of nucleation, collision–coalescence, collection, and gravitational settling would not be hidden by nudging, but errors in the treatment of radiative heating, condensation/vapor deposition, evaporation/sublimation, melting, cumulus convection, and subgrid or resolved transport of heat and moisture would be hidden by nudging.

1. Introduction

The climate modeling community is developing a revolutionary suite of cloud parameterizations with the hope that the added complexity of cloud microphysics will reduce uncertainty in estimates of climate sensitivity and climate change. These cloud parameterizations predict cloud liquid water and, in some schemes, cloud ice. Parameterizations of cloud radiative properties have also been developed to treat the impact of the clouds on the radiation balance.

Almost without exception, evaluation of these cloud parameterizations has relied upon comparison of simulated and observed climatological (usually monthly) means of the earth radiation budget or liquid water path. Comparison on shorter timescales is seldom attempted, partly because quantitative global information cannot be obtained on shorter timescales from the polar-orbiting satellites used to provide global observations, and partly because natural variability obscures model errors on shorter timescales.

Recent advances in the use of geostationary platforms as a source of quantitative high time resolution cloud and radiation observations (Minnis et al. 1995), together with the deployment of high-density, surface-based, research quality radiometric and meteorological instruments (Stokes and Schwartz 1994), now provides data that can be used to evaluate cloud parameterizations on much shorter timescales, from minutes to weeks. A much richer set of observations is now available to the climate modeling research community.

However, selection of an appropriate modeling strategy that takes advantage of these new data is far from obvious. Clearly any cloud parameterization testbed for shorter timescales must be constrained by observed winds so that errors due to the cloud parameterization can be distinguished from differences due to natural

Corresponding author address: Dr. Steven J. Ghan, Pacific Northwest National Laboratory, Battelle Boulevard, P.O. Box 999, Richland, WA 99352.
E-mail: steve.ghan@pnl.gov

variability. The single-column model (SCM) has been promoted as a useful testbed for cloud parameterizations (Randall et al. 1996), but providing the necessary lateral boundary conditions has proven to be extremely challenging because of sampling and measurement errors in the winds (Zhang and Lin 1997; Mace and Ackerman 1996; Randall et al. 1996) and because of the lack of cloud measurements along the lateral boundaries (Petch and Dudhia 1998). Use of a regional circulation model to provide lateral boundary conditions for an SCM introduces dependencies upon the particular treatment of clouds in the regional model.

Here we consider two alternatives to the single-column modeling strategy. The first expands the modeling domain so that it is large enough that the lateral boundary conditions for the cloud variables are unimportant for the smaller validation region; previous work by Westphal et al. (1996) indicates that a domain of at least 1000 km is necessary for strongly advected high cirrus clouds. Because this is much larger than the size of a single global circulation model (GCM) grid cell, a multidimensional regional circulation model (RCM) is necessary for such a domain. By predicting the circulation within its domain, the circulation in an RCM is less sensitive to errors in the lateral boundary conditions than in an SCM because the model dynamics permit geostrophic adjustment. Moreover, by predicting the cloud variables throughout the model domain, the lateral boundary conditions for the clouds in the validation region are dependent upon the same treatment of cloud microphysics outside the validation region as within, thus eliminating inconsistencies between the treatment of clouds in an SCM and in a regional model providing its lateral boundaries.

The second alternate strategy is to constrain a GCM with observed winds through some form of data assimilation (Jeuken et al. 1996). Although the results can be sensitive to the particular data assimilation scheme employed, this approach has the advantage that it can be applied to the particular GCM for which the cloud parameterization is being developed. However, because the domain is global this testbed consumes more computer resources than regional testbeds.

Each modeling strategy offers advantages and disadvantages. The SCM is computationally very fast, but is extremely sensitive to its lateral boundary conditions, which control vertical velocity and horizontal advective tendencies of temperature and moisture. An RCM is faster than a GCM, is less sensitive to lateral boundary conditions than an SCM, and (because of the influence of its lateral boundary conditions) is less sensitive to data assimilation than a GCM, but care must be taken to ensure that it uses the same treatment of physics as in the GCM for which the cloud parameterization is being developed. A GCM is self-consistent with its cloud parameterization and has no lateral boundary conditions, but it is slower and can be sensitive to the data assimilation scheme.

Other strategies for evaluating cloud and radiation parameterizations involve using high-resolution cloud-resolving models to produce a synthetic database. These strategies are being developed under the Global Energy and Water-Cycle Experiment (GEWEX) Cloud System Study (GCSS Science Team 1993; Moncrief et al. 1997).

In this paper we compare and contrast results from the single-column, regional, and global modeling strategies for a particular period, namely 24 October–14 November 1994, and for a particular region, namely the Atmospheric Radiation Measurement (ARM) Southern Great Plains (SGP) Clouds and Radiation Testbed (CART). The focus is not on absolute model performance, but rather on whether the performance of one test bed is indicative of the performance of the other test beds. Section 2 describes the experiment design and the particular models and parameterizations. Section 3 describes the data used in the evaluation. Section 4 compares the simulated and observed fields. Conclusions are drawn in section 5.

2. Experiment design

The purpose of this investigation is to compare and contrast three different modeling strategies for evaluating cloud parameterizations. Such a comparison can only be meaningful when the three different models resemble each other as closely as possible in all respects except those related to the different strategies. Thus, all three models are run at the same resolution and with the same treatment of physical processes.

The global circulation model (GCM) is derived from the National Center for Atmospheric Research (NCAR) Community Climate Model (CCM2). For this study we have replaced the NCAR CCM2 treatment of stratiform clouds (Kiehl et al. 1994) with a simplified form of the Colorado State University (CSU) Regional Atmospheric Modeling System (RAMS) bulk microphysics parameterization (Ghan and Easter 1992; Ghan et al. 1997), assuming the stratiform cloud fraction is unity whenever condensed water is predicted. The prognostic variables temperature T and water vapor mixing ratio r_v have been replaced by the condensation-conserved variables $T_c \equiv T - L/c_p r_c$ and $r_w \equiv r_v + r_c$, so that the cloud water mixing ratio r_c is diagnosed from T_c and r_w assuming condensation instantaneously eliminates supersaturation with respect to liquid water. Water (r_w and cloud ice) is transported using the semi-Lagrangian scheme of Williamson and Rasch (1994). The radiative properties of convective clouds are neglected, while stratiform cloud radiative properties are related to the number and mass concentrations of cloud droplets and ice crystals. Droplet number density is prescribed at 100 cm^{-3}. The NCAR CCM2 treament of subgrid boundary layer transport (Holtslag and Boville 1993) is retained, but the NCAR CCM2 treatment of land surface processes is replaced by the Biosphere–Atmosphere Transfer Scheme (BATS) 1E of Dickinson et al. (1993). Nudging

of temperature and winds has been added to constrain the simulation toward the European Centre for Medium-Range Weather Forecasts (ECMWF) T42 6-hourly analysis, using nudging coefficients of 2.5×10^{-5} s^{-1} above the boundary layer and zero within the boundary layer. Note that the humidity is not nudged because that would compromise the independent evaluation of the cloud parameterization. Temperature is nudged for geostrophic consistency with the nudging of the wind components. Although nudging temperature affects the humidity field, it should have much less effect on the cloud fields than nudging both temperature and humudity because nudging only one of these fields allows the model to use its own criterion for condensation. The values of the nudging coeffients have been selected on the basis of sensitivity experiments balancing the need to force the simulated winds toward observations with the need to keep the nudging terms from becoming the dominant terms in the conservation equations (Jeuken et al. 1996).

The RCM is derived from the nonhydrostatic version of the Pennsylvania State University–National Center for Atmospheric Research Mesoscale Model version 5 (MM5) (Grell et al. 1993). For this study we have replaced the MM5 treatment of stratiform clouds with the same simplified form of the CSU RAMS bulk microphysics parameterization described by Ghan et al. (1997), and have replaced the prognostic variables T and r_v with T_c and r_w. Water (r_w and cloud ice) is transported using the centered finite-difference method for horizontal transport and using a harmonic mean finite-difference method for vertical transport. The treatment of solar and longwave radiative transfer has been replaced by the treatment in the NCAR CCM2. The radiative properties of convective clouds are neglected, while stratiform cloud radiative properties are related to the number and mass concentrations of cloud droplets and ice crystals in the same way as in the GCM. The treatment of moist convection is replaced by the CCM2 Hack (1994) scheme. The treatment of subgrid boundary layer transport is replaced by that in the NCAR CCM2, and the treatment of land surface processes is replaced by the BATS 1E scheme. Thus, the treatment of all physical processes in this version of MM5 should be identical to that in the GCM. The same treatment of nudging as in the GCM is also applied to the RCM, interpolating the ECMWF analysis from the ECMWF T42 grid to the RCM grid.

The SCM is essentially a single column of the GCM, but with vertical velocity and lateral boundary conditions prescribed rather than interacting with adjacent columns. The same code is used in both the SCM and GCM, except for the prediction of winds (which are prescribed from observations in the SCM) and the treatments of horizontal advection (which is prescribed from observations in the SCM) and horizontal diffusion (which is neglected in the SCM). Thus, as we shall demonstrate, if the winds and advective tendencies used to drive the SCM are the same as those simulated by the GCM, the SCM and GCM will yield virtually the same simulation of clouds and radiative fluxes.

Each of these models has different input requirements. The SCM requires time series of vertical profiles of vertical velocity, wind speed, temperature, water vapor, and horizontal advective tendencies of temperature and water vapor, averaged over a domain the same size as a GCM grid cell. In some simulations the vertical profiles of temperature and water vapor are used to treat the feedback of the simulated temperature and water vapor on the horizontal advection of those fields; nudging of simulated temperature and water vapor toward the observed fields is applied, using the advective timescale for the nudging coefficient. The advective timescale is based on the observed wind speed and an assumed GCM grid scale of 300 km. All of the input fields are from Zhang and Lin's (1997) variational analysis of ARM SGP measurements, which adjusts the vertical profiles of vertical velocity, temperature, water vapor, and horizontal advective tendencies of temperature and water vapor to ensure that the column mass, energy, and moisture budgets are consistent with measurements at the surface and at the top of the atmosphere. The soil temperature is initialized with the observed surface air temperature. The soil moisture is initialized at the BATS field capacity, defined such that gravitational drainage is 2 mm day^{-1}. The vegetation type and soil texture are taken from the values of the closest T42 GCM grid cell to the SGP site, that is, at 37.7°N and 98.4°W, using the same database used by the GCM. The ozone profile is taken from the GCM ozone database for the closest T42 latitude band.

The RCM requires time series of surface pressure and of vertical profiles of horizontal winds, temperature, and water vapor along its lateral boundaries. In addition, it needs time series of analyzed surface pressure, horizontal winds, and temperature within its interior to treat initialization and nudging. These time series are interpolated to the RCM grid from the ECMWF T42 6-hourly analysis. Soil temperature is initialized at the analyzed surface air temperature. The soil moisture is initialized in the same manner as in the SCM. The vegetation type/land use is taken from the MM5 terrain database, converted to comparable BATS types (differences from the CCM BATS database are small); soil texture is interpolated from the BATS T42 dataset.

The GCM has no lateral boundary conditions but needs global gridded time series of analyzed surface pressure, horizontal winds, humidity, and temperature to treat initialization and nudging. These are interpolated to the GCM vertical coordinate levels from the same ECMWF analysis. Soil temperature and soil moisture are initialized in the same manner as in the RCM.

Because each of these models employs different coordinate systems, it is not possible to run the models with identical spatial resolution. The GCM is run at T42 spectral resolution, corresponding to about 2.8° lat × 2.8° long grid resolution for the model physics. The

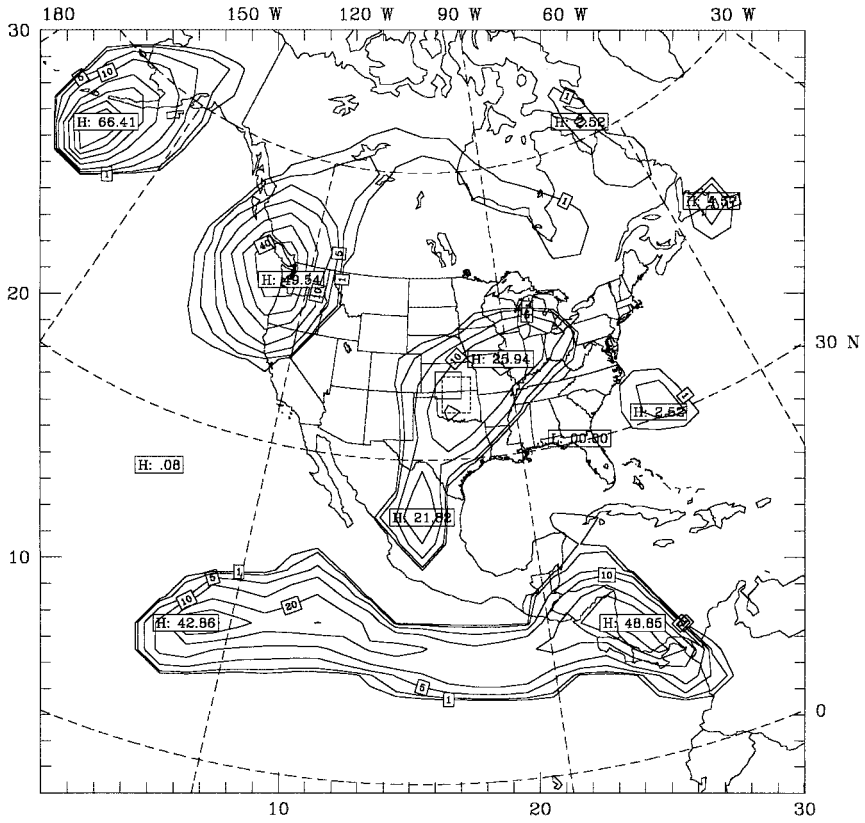

FIG. 1. Spatial distribution of the daily mean precipitation rate on 4 Nov 1994 as simulated by the RCM. Contour levels are 1, 2, 5, 10, 20, and 50 mm day^{-1}. The bounds of the ARM CART domain are indicated by the dashed line over Oklahoma and Kansas. The grid cell for the analysis of the RCM results is indicated by the solid box centered over southern Kansas. The grid cell for the analysis of the GCM results is centered at the same point.

RCM is run at 300-km resolution for a domain spanning the entire continental United States (Fig. 1); the Lambert conformal projection grid is centered at the same point as the GCM grid closest to the SGP central facility, that is, at 37.7°N and 98.4°W. The SCM has a horizontal grid size of 300 km implicit in the treatment of advective nudging and in the analysis of the input variables. All three models are run with 24 levels, with 9 levels in the lowest 15% of the atmosphere; however, the RCM uses the σ vertical coordinate in which $p = p_t + \sigma(p_s - p_t)$ with $p_t = 10^2$ Pa, while the GCM and SCM use the hybrid vertical coordinate η in which $p = A(\eta)p_0 + B(\eta)p_s$. Although the σ levels in the RCM have been chosen to correspond to the values of $A(\eta) + B(\eta)$ in the GCM and SCM such that the vertical levels in the RCM match those in the GCM and SCM when $p_s = p_0 = 10^5$ Pa, for other values of the surface pressure p_s the vertical levels of the RCM and GCM/SCM will differ somewhat.

The selected period for this comparison is 25 October–10 November 1994. This is an ARM intensive observation period (IOP), in which radiosondes were launched every 3 h at the SGP central facility and at four boundary stations. The RCM and GCM are both initialized at 0000 UTC 24 October 1994, and are run to 0000 UTC 14 November 1994. All results shown are for the grid cell closest to the SGP central facility, which is centered about 100 km away, that is, at 36.6°N and 97.5°W.

3. Observations

The observations used to evaluate the model simulations consist of earth radiation budget estimates from National Oceanic and Atmospheric Administration (NOAA) Geostationary Operational Environmental Satellite (*GOES-7*) measurements, surface radiation budget measurements by ARM solar and infrared radiation observation stations (SIROS), surface sensible and latent heat flux measurements by energy balance Bowen ratio (EBBR) stations, estimates of column water vapor and column cloud liquid water from microwave radiometer (MWR) measurements, and precipitation measurements at 47 Oklahoma Mesonet and 5 surface meteorological observing system (SMOS) stations.

The *GOES-7* visible and infrared radiance measurements have been converted to hourly 0.5° lat × 0.5° long gridded broadband fluxes by Minnis et al. (1995).

The flux estimates were then averaged over the 365 km × 300 km CART domain.

The SIROS instruments consist of pyranometers to measure the downwelling and upwelling hemispheric solar flux and of pyrgeometers to measure the downwelling and upwelling hemispheric broadband infrared flux. SIROS instrumentation is deployed at four extended facilities within the CART domain. Area and hourly means of the 15-s measurements are formed from simple arithmetic means of the available observations, filtering out values outside the geophysically realistic bounds of 10–600 W m^{-2} for downwelling and upwelling infrared flux, −10 to 1600 W m^{-2} for downwelling solar flux, and −10 to 100 W m^{-2} for upwelling solar flux.

Hourly CART-area mean precipitation rates were formed from the 5-min Oklahoma Mesonet and 30-min SMOS measurements.

Surface fluxes of sensible and latent heat were measured every 30 min by a suite of 10 EBBR stations located at the central and extended CART facilities. CART domain means were formed after outlier values were discarded from the individual station data.

Hourly means of column water vapor and column cloud liquid water were formed from 5-min averages of estimates from microwave radiometer measurements at the central and two boundary CART facilities. Uncertainty in the column water vapor and cloud liquid water is estimated to be 0.05 cm and 30 g m^{-2}, respectively (Lesht and Liljegren 1997). Data is treated as missing when rain is standing on the instrument.

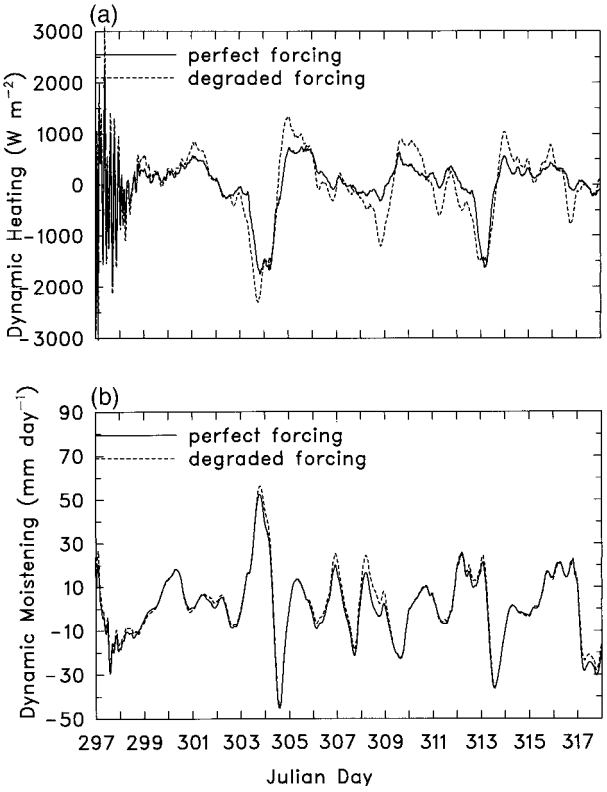

FIG. 2. Column-integrated (a) dynamical heating and (b) dynamic moistening simulated by the GCM (perfect forcing) and degraded by amplifying the vertical velocity and divergence by 20%.

4. Results

a. SCM driven by GCM

Before comparing the simulations with observations, we first establish the SCM as a useful testbed by comparing a GCM simulation with SCM simulations driven by GCM forcing. The GCM is driven by the ECMWF analysis for the experiment period described in section 2. The SCM is driven by the GCM horizontal and vertical components of velocity, surface pressure, horizontal advective tendencies of temperature, water vapor + cloud water, and cloud ice, and the GCM nudging term for temperature. All of these fields are archived from the GCM simulation every time step at the grid cell closest to the ARM CART site. Nudging of temperature and humidity toward the GCM ''observations'' are turned off. From these fields, the SCM calculates vertical advective tendencies, all physical processes, and predicts temperature, water vapor + cloud water, cloud ice, surface temperature, and soil moisture. Because almost all of the SCM code is identical to the GCM code, SCM simulations driven by GCM forcing should agree almost perfectly with the corresponding GCM simulation; the simulations are in fact virtually indistinguishable, so we do not illustrate them here. However, we have found that the agreement is achieved only if considerable care is exercised in determining the appropriate forcing for the SCM. In particular, the forcing must account for the spectral truncation of the diabatic heating (which is calculated in gridpoint space) in the GCM time integration sequence. This is done by simply determining the horizontal advective tendency of temperature as a residual in the GCM heat budget, so that it implicitly accounts for the spectral truncation of the diabatic heating.

If the SCM is to be driven by observations, we need to understand its sensitivity to forcing so that we can reconcile differences between SCM and GCM simulations. To determine the sensitivity of the SCM, we have performed several experiments using GCM forcing. First, we drive the SCM with GCM forcing degraded somewhat by amplifying the vertical velocity and divergence fields by 20%. Such an error is probably less than what might be expected for a 300-km square region covered with a relatively dense network of observations. Figure 2 compares the column-integrated dynamic heating (total advection of heat, plus adiabatic expansion) and dynamic moistening (total advection of moisture) for the perfect forcing and degraded forcing SCM simulations. The dynamic heating is initially very noisy because the initial conditions are not in geostrophic bal-

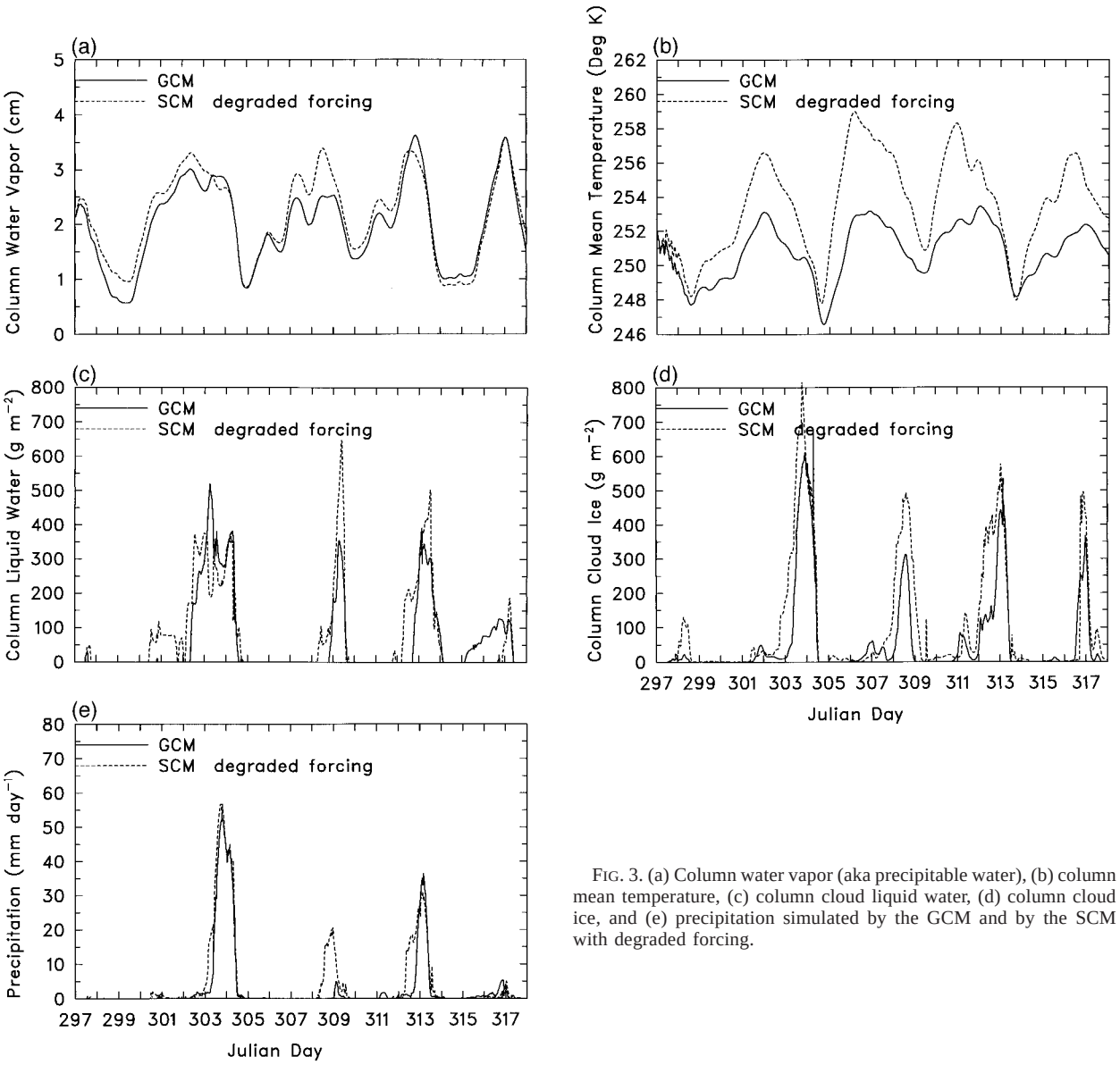

FIG. 3. (a) Column water vapor (aka precipitable water), (b) column mean temperature, (c) column cloud liquid water, (d) column cloud ice, and (e) precipitation simulated by the GCM and by the SCM with degraded forcing.

ance. After two days the dynamic heating settles down, with differences of typically 300 W m^{-2}, smaller than the dynamical heating, but as we shall see comparable to the heating due to physical processes. Differences in the dynamic moistening are typically less than 5 mm day^{-1}, much smaller than the dynamic moistening, but comparable to the physical moistening. Consequently, the SCM and GCM simulations of water vapor, temperature, clouds, and precipitation, illustrated in Fig. 3, diverge within just a few days. Although the SCM continues to simulate the timing of the cloud systems correctly, it also simulates spurious clouds and yields significant errors in the clouds whose timing is simulated correctly.

How can such differences be corrected? One approach is to allow the horizontal advection of the temperature and humidity to depend upon the temperature and humidity of the single column. That is, we use upstream differencing to express the horizontal advective tendency H of variable ψ in terms of an upstream value ψ_u, the value simulated by the SCM ψ_m, and the advective timescale $\tau_a = \Delta x V^{-1}$:

$$H(\psi) = \frac{\psi_u - \psi_m}{\tau_a}, \tag{1}$$

where Δx is the SCM grid size and V is the wind speed. The upstream value can be determined by using upstream differencing to express the ''observed'' horizontal advective tendency A in terms of the upstream value and the value of ψ ''observed'' in the column:

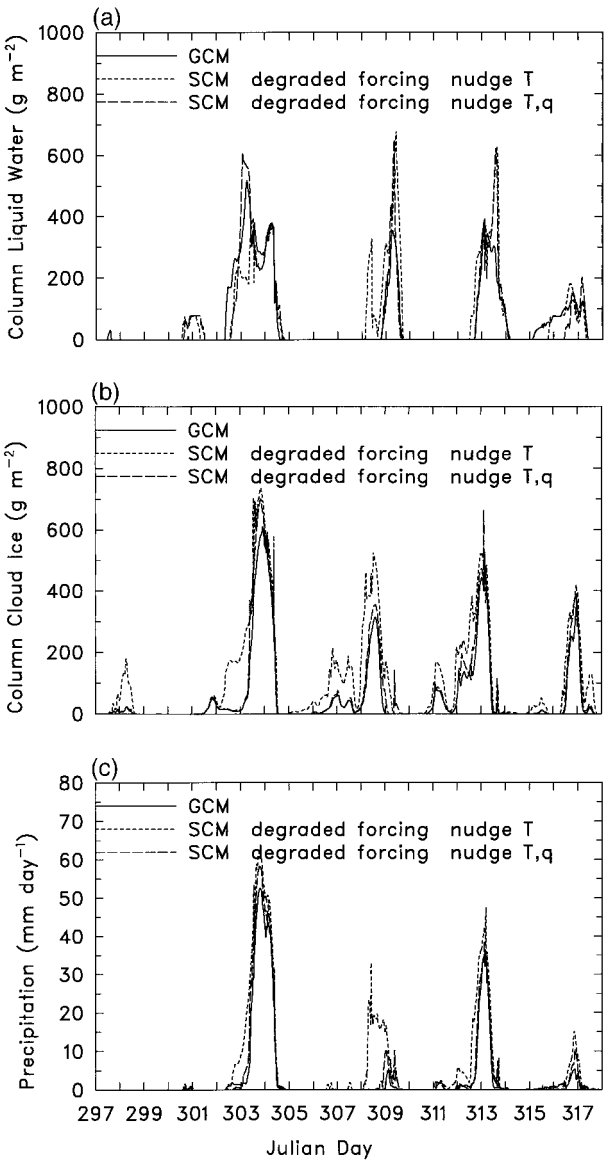

FIG. 4. (a) Column cloud liquid water, (b) column cloud ice, and (c) precipitation simulated by the GCM, by the SCM with degraded forcing and advective nudging of temperature and water vapor, and by the SCM with degraded forcing and advective nudging of temperature only.

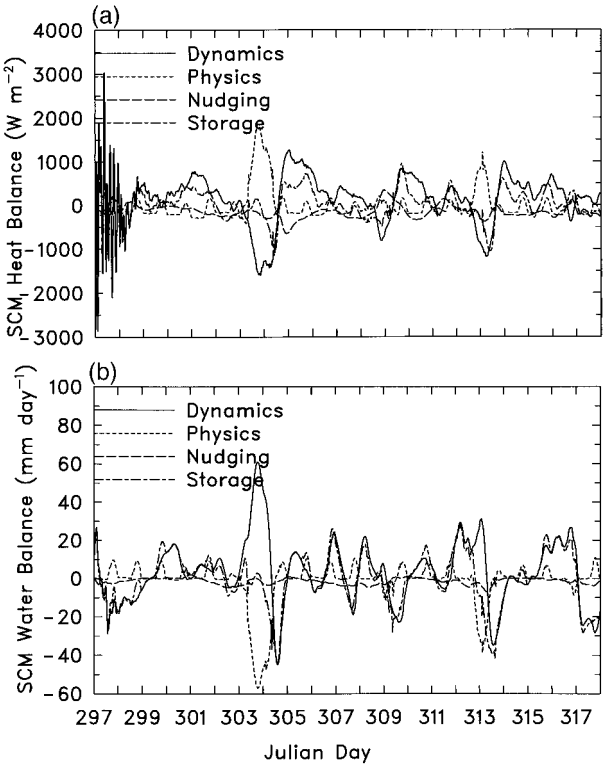

FIG. 5. (a) Column mean heat balance and (b) moisture balance of SCM simulation with degraded forcing and advective nudging of temperature and water vapor, comparing the tendency due to large-scale dynamics (advection and adiabatic cooling), physical processes (surface fluxes, condensation, evaporation, and radiative cooling), advective nudging, and total storage.

$$A(\psi) = \frac{\psi_u - \psi_o}{\tau_a}, \tag{2}$$

so that

$$\psi_u = \psi_o + A(\psi)\tau_a. \tag{3}$$

Substituting (3) in (1) yields

$$H(\psi) = A + \frac{\psi_o - \psi_m}{\tau_a}. \tag{4}$$

In other words, to treat the feedback of the simulated temperature and humidity on their horizontal advective tendencies, we simply retain the ''observed'' horizontal advective tendencies and nudge the simulated temperature and humidity toward their ''observed'' values. Thus, adding nudging toward ''observed'' values is equivalent to adding feedback of the SCM simulated values on the horizontal advection.

To see the impact of nudging, Fig. 4 compares the GCM simulation with an SCM simulation with degraded forcing and with temperature and water vapor nudged toward the GCM values. The agreement for cloud liquid water, cloud ice, and precipitation is much better with than without nudging. This suggests that nudging can provide an effective means of correcting simulations degraded by errors in the larger-scale forcing of temperature or water vapor.

One criticism of nudging is that it introduces a spurious term in the budgets of the nudged fields. Figure 5a compares the column mean heating due to nudging with that due to dynamics (horizontal advection, vertical advection, and adiabatic expansion), physics (surface sensible heat flux, latent heat release, radiative flux convergence), and storage (temperature tendency) in the degraded SCM simulation with nudging of temperature and humidity. The dynamics term is large during the

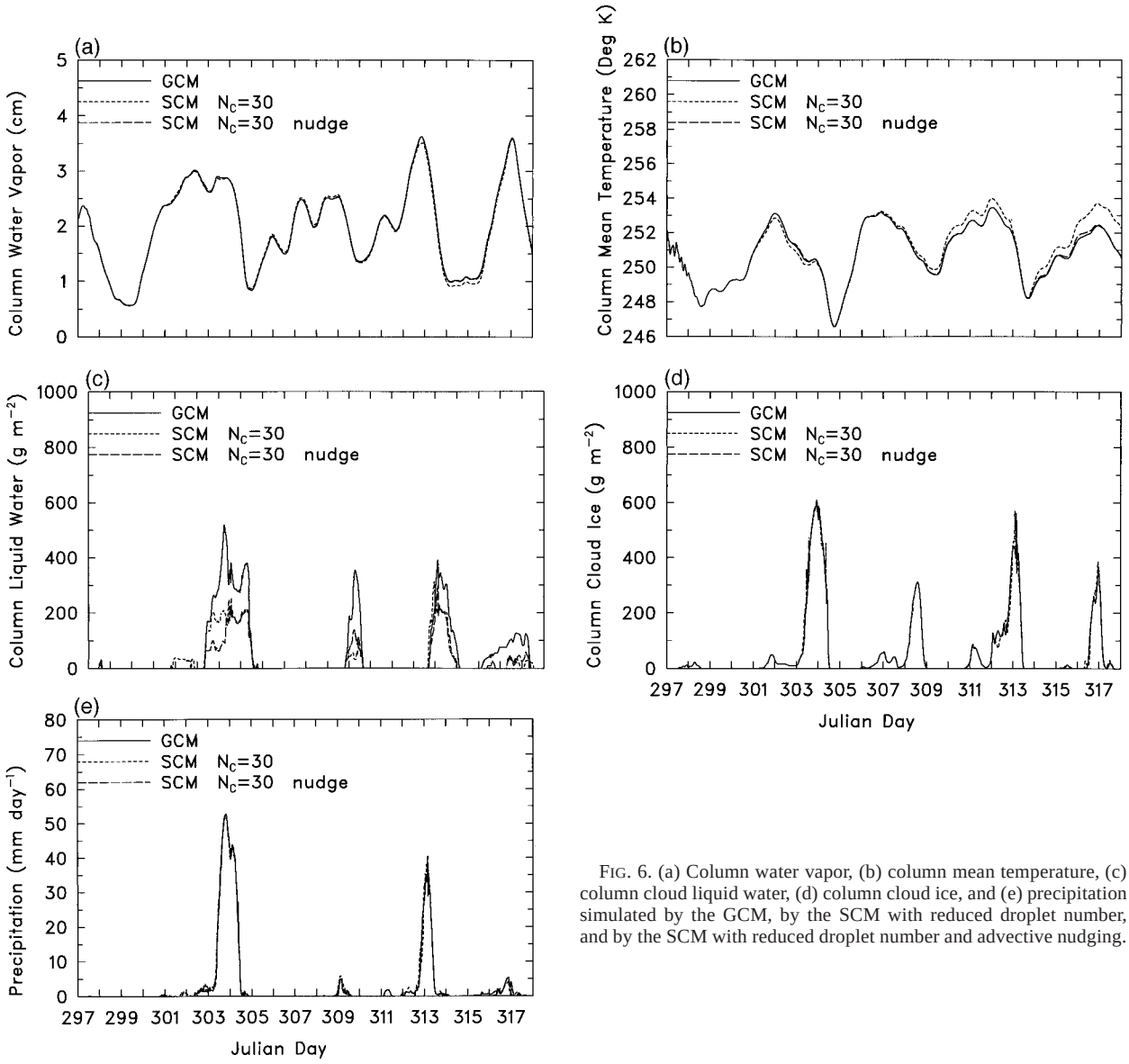

FIG. 6. (a) Column water vapor, (b) column mean temperature, (c) column cloud liquid water, (d) column cloud ice, and (e) precipitation simulated by the GCM, by the SCM with reduced droplet number, and by the SCM with reduced droplet number and advective nudging.

first two days as the GCM simulation used to drive the SCM adjusts to the initial geostrophic imbalance. The nudging term is usually the smallest term in the column heat budget, yet it can be as large as 300 W m^{-2} at times. Figure 5b compares the column mean moistening due to nudging with that due to dynamics (horizontal and vertical advection), physics (surface water vapor flux, condensation, and evaporation), and storage (moisture tendency) in the degraded SCM simulation with nudging. The nudging term is usually the smallest term in the column moisture budget, never exceeding 5 mm day^{-1}. If errors in the forcing are larger, the nudging terms would be proportionately larger as well.

Another criticism of nudging is that it can hide errors in model physics. To address this issue, we drive an SCM with ''perfect'' GCM forcing but with ''degraded'' physics. We consider two types of physics degradation, one involving physics that does not directly influence the nudged fields (temperature and humidity), the second involving physics that does. In the first case, we simply reduce the assumed droplet number concentration from 100 to 30 cm^{-3}. Doing so is likely to influence cloud water and perhaps also precipitation, but not temperature or water vapor. If temperature and water vapor are unchanged by the physics degradation, then nudging of temperature and humidity will have no influence on the simulation, and hence will not hide the influence of the droplet number ''error'' on other fields. We run two degraded SCM simulations, one with and one without nudging. Figure 6 compares the degraded SCM simulations with the perfect GCM simulation. As expected, neither simulation yields significantly different water

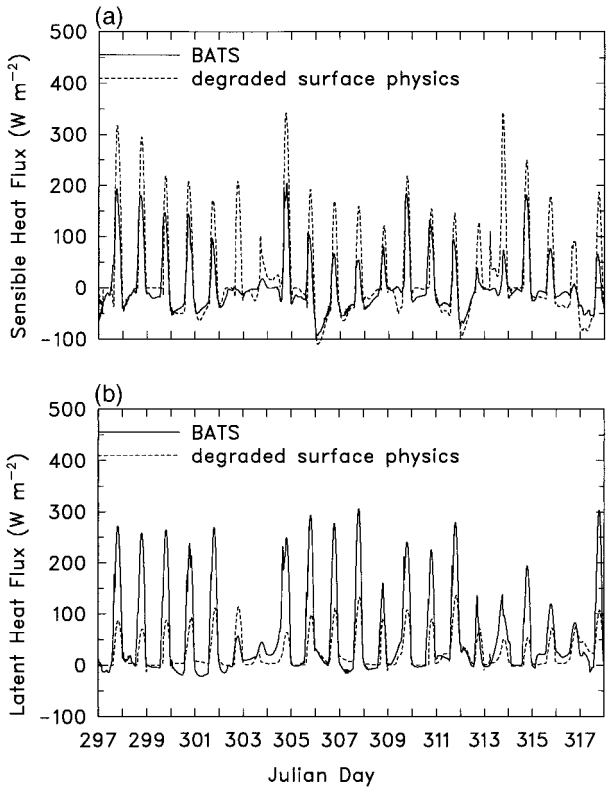

FIG. 7. (a) Surface sensible and (b) latent heat flux simulated by the GCM with BATS (solid line) and by the SCM without BATS (dashed line).

vapor or temperature, and both SCM simulations yield significantly lower cloud water concentrations than the perfect control. There is little evidence that nudging hides the impact of the lower droplet number on cloud water. The degraded droplet number has little impact on cloud ice or precipitation.

If the degraded physics directly influences temperature and water vapor, then it is much more likely that nudging temperature and water vapor will hide the degraded physics. To illustrate this, we degrade physics by replacing the BATS surface physics with the NCAR CCM2 treatment of surface physics. Figure 7 compares the perfect GCM-simulated surface fluxes with the degraded SCM simulation. Persistent differences in the surface fluxes are evident, with BATS predicting generally lower sensible heat flux and higher latent heat flux than the NCAR CCM2 treatment. These differences directly influence the atmospheric temperature and humidity. Figure 8 compares the perfect GCM simulated water vapor, temperature, and clouds with degraded SCM simulations with and without nudging. In the absense of nudging, the atmosphere is consistently warmer and drier in the simulation with the NCAR CCM2 treatment of surface fluxes. Consequently, cloud formation is substantially reduced in the degraded simulation without nudging; cloud water is delayed a full day on day 303 and is completely missed on day 309 and days 316–317. When nudging is applied to the degraded model, cloud water forms at the correct time on day 303 and forms on day 309, albeit weaker than in the control simulation. The timing of precipitation is also improved when nudging is applied. These results suggest that nudging can hide errors in the treatment of surface physics. On the other hand, if the focus of the investigation is on evaluating a stratiform cloud microphysics parameterization, then hiding such errors can be considered an advantage of nudging.

To conclude this section, we have found that nudging of temperature and humidity in an SCM can reduce the influence of errors in the large-scale forcing, but it can also hide errors in model physics. However, physics errors are hidden by nudging only if the errors impact temperature or humidity. Thus, errors in the treatment of nucleation, collision–coalescence, collection, and gravitational settling would not be hidden by nudging, but errors in the treatment of radiative heating, condensation/vapor deposition, evaporation/sublimation, melting, cumulus convection, and transport (subgrid or large-scale) of heat and moisture would be hidden. Although the errors in the treatment of some of these processes may be small, errors in the treatment of many processes are potentially large enough to seriously degrade the cloud simulation. Moreover, there are limits to how much nudging can reduce the influence of errors in large-scale forcing; if the sign of the vertical velocity is incorrect then nudging can improve the humidity fields but it will not necessarily improve the cloud fields.

b. SCM, RCM, GCM driven by observations

We now compare a variety of simulated cloud-related fields with observations. To facilitate comparison, we compare only daily means of each field. At the spatial scale of a GCM grid cell (300 km) one cannot expect agreement between models and observations on time scales much shorter than one day. Averaging fields each day reduces the degrees of freedom in the data, but also permits easier detection of systematic differences.

Again we remind the reader that our focus is not on absolute performance but rather on the question of whether the performance of one test bed is indicative of the performance of the other test beds. With a horizontal resolution of 300 km, no subgrid treatment of clouds, and with the closest grid point to the CART site 100 km away, one should not expect these simulations to agree with observations as well as simulations with much finer spatial resolution. The question we are addressing is whether simulations with the same resolution and physics but different domain sizes can agree well enough at a single grid point that biases evident in one test bed simulation are also evident on the others.

To facilitate comparison between the SCM simulation and the simulations by the RCM and GCM, nudging in the SCM is applied to temperature but not humidity. By

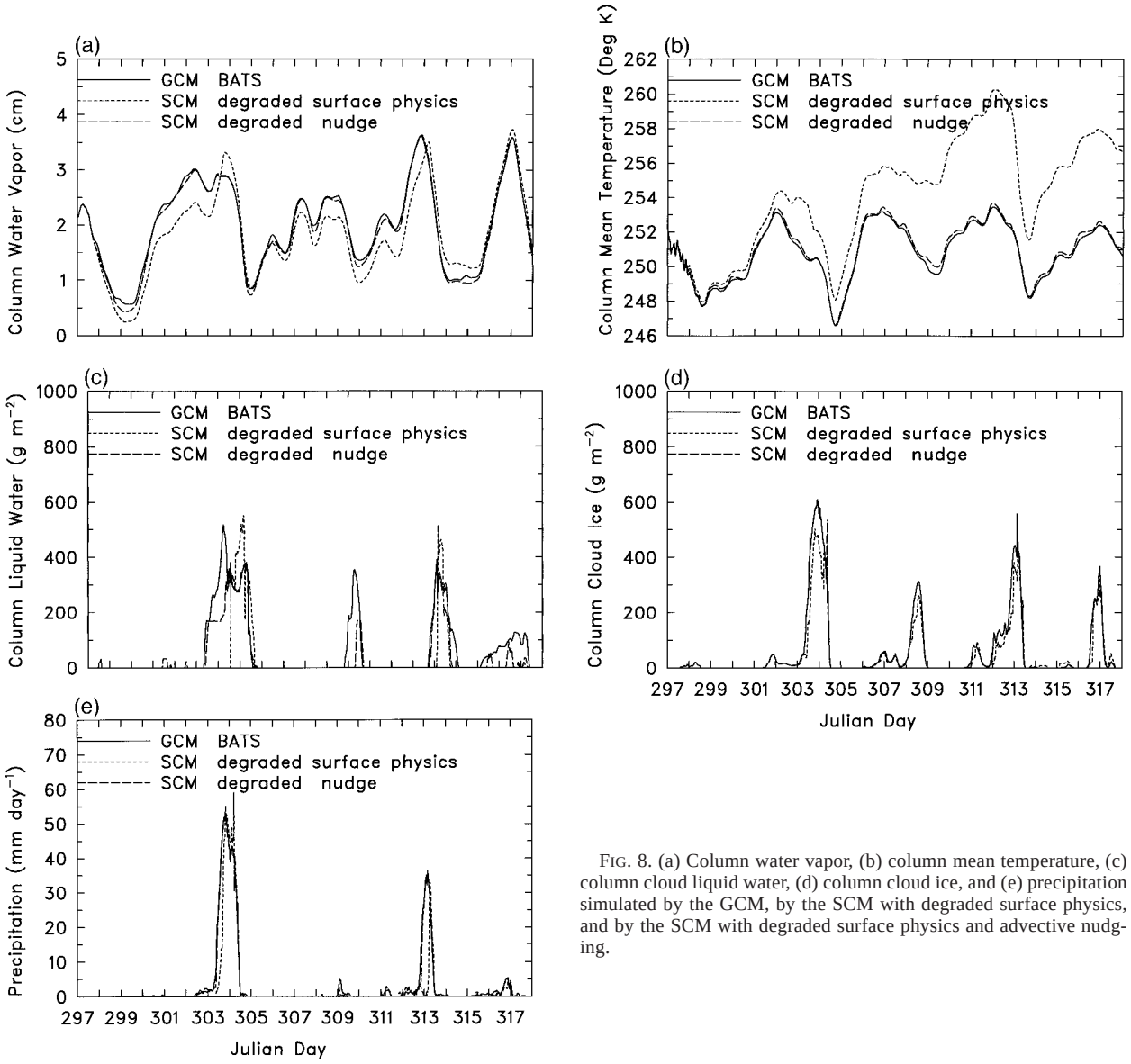

FIG. 8. (a) Column water vapor, (b) column mean temperature, (c) column cloud liquid water, (d) column cloud ice, and (e) precipitation simulated by the GCM, by the SCM with degraded surface physics, and by the SCM with degraded surface physics and advective nudging.

omitting nudging of humidity in all three models, the impact of physics errors on humidity and clouds is less likely to be hidden, and differences between the SCM simulation and RCM and GCM simulations can be attributed to differences in the forcing. However, errors in the large-scale forcing are more likely to produce errors in the humidity and cloud fields if humidity is not nudged. To see this, Fig. 4 also shows an SCM simulation with degraded GCM forcing and with only temperature nudged toward the GCM value. The simulation with nudging of humidity as well as temperature is clearly superior to the simulation with nudging of temperature only, even though according to Fig. 2b the ''error'' in the moisture forcing is small. Thus, when the simulation of a particular variable by the SCM is particularly poor, we will refer to an SCM simulation with humidity nudging to determine to what extent humidity nudging can correct (hide) the bias.

Figure 9a compares the column water vapor measured at the SGP site with that simulated by the GCM, RCM, and SCM for the period 24 October–13 November 1994 (the SCM simulation is restricted to the period 25 October–9 November). Although all three models simulate the timing of the moist and dry episodes quite well, persistent moist biases of up to 80% are evident in each simulation. At most times the differences between simulations are less than the differences between simulation and observation, which suggests deficiencies in model physics are larger factors in the biases than are uncertainties in forcing (note that the SCM is driven by the Zhang and Lin objective analysis, whereas the RCM and GCM are driven by the ECMWF analysis). Thus,

at least for water vapor the RCM and the SCM are useful test beds for identifying a deficiency in the GCM.

Figure 9b compares the simulated and observed column cloud liquid water. Again, all three models simulate the timing of the cloud systems quite well. For the first cloud system on Julian days 303–304 the GCM simulates about 40% more cloud water than observed or simulated by the other models. The SCM captures the magnitude of the column liquid water in the first cloud system quite well, but the cloud water forms about one day too early. The RCM and GCM simulate the amount of column liquid water in the second cloud system quite well, but the timing differs by 12 h between models; the SCM simulates twice as much cloud water as observed for the second cloud system. In the third cloud system on days 313 and 314, the SCM simulates about three times as much cloud water as observed, the GCM simulates about 50% more than observed, and the RCM about 60% of observed. Differences between the RCM and GCM cloud water are typically a factor of 2, with the GCM simulating more cloud water for most but not all cloud systems. If the SCM humidity is nudged toward the Zhang and Lin humidity analysis the moist bias in relative humidity is reduced so that the simulated cloud water is much more realistic and closer to that simulated by the RCM and GCM. The cloud water simulated by the SCM forced by data constrained only by the column mass budget is also unrealistic.

Although observations of cloud ice are not available, Fig. 9c compares the column cloud ice simulated by the three models so that the simulated radiation fields can be understood later. The column cloud ice simulated by the RCM is generally in good agreement with that simulated by the GCM, with excellent agreement in the timing of the cloud systems and differences in the magnitude of usually less than 40%. For the first cloud system the SCM simulates about half as much cloud ice as the RCM and GCM, but agreement is much better for the second and third cloud systems. When the SCM simulation is nudged toward the observed humidity the relative humidity is reduced, so that the simulated cloud ice is less than half of that simulated by the RCM and GCM.

Figure 9d compares the observed precipitation rate with that simulated by the three models. Consistent with the cloud simulation, all three models simulate the timing of the precipitation quite well. However, the three models yield quite different precipitation amounts. For the first cloud system both the RCM and GCM simulate about twice as much precipitation as observed, while the SCM simulates the peak daily precipitation rate very well but starts the precipitation two days too soon. Weather summaries at the CART site indicate a squall line produced the precipitation on day 304 (31 October), but almost all of the precipitation simulated by the RCM and GCM and most of that simulated by the SCM was from stratiform clouds. For the second cloud system the SCM again simulates the peak daily precipitation rate very well, while the RCM simulates about 60% of observed precipitation and the GCM simulates less than 10% of that observed. Weather summaries again indicate much of the precipitation on day 309 was from thunderstorms, but that most of the precipitation simulated by the RCM and SCM is from stratiform clouds. For the third cloud system the RCM simulates about twice the observed precipitation and SCM and GCM both about 50% more than observed. For the fourth cloud system the GCM simulates somewhat less precipitation than observed, and the RCM about 50% more. An SCM simulation with nudging of humidity yields much weaker precipitation rates in the first and third cloud systems because the cloud ice is greatly reduced. The precipitation simulated by the GCM in the second cloud system is weak because the cloud ice is simulated prior to, rather than concurrent with, the cloud water, so that the seeder-feeder mechanism cannot operate.

The differences in model simulations of cloud water and cloud ice are reflected in the solar fluxes at the surface and top of the atmosphere. Figure 9e compares the simulated and observed outgoing shortwave flux at the top of the atmosphere. The models capture the maximum outgoing shortwave flux associated with the first cloud system fairly well, overestimating the flux by about 30 W m^{-2}. All three models largely miss a secondary maximum in the flux on day 306, but capture the large maximum on day 309 quite well. Although the flux simulated by the SCM and GCM is about 50 W m^{-2} larger than that simulated by the RCM for days 302–303, it is about 20 W m^{-2} smaller for days 306–308. All three models overestimate the flux by 40 W m^{-2} on day 312. On day 313 the SCM and GCM continue to overestimate the flux, consistent with their excessive simulated cloud water.

The downward shortwave flux at the surface (Fig. 9f) mirrors the upward flux at the top of the atmosphere. The models simulate the minimum in the downward flux on day 303 quite well, but consistent with Fig. 9e the models overestimate the flux on days 305–306. The models capture the timing of the minimum of the flux on day 308, but the flux simulated by the GCM exceeds that simulated by the SCM and RCM by more than 60 W m^{-2}. Note that the cloud system on day 313 is evident in both the simulated and observed downward flux at the surface, but not in the observed upward flux at the top of the atmosphere.

The outgoing longwave flux at the top of the atmosphere is most sensitive to upper-tropospheric water vapor and (ice) clouds. Figure 9g reveals a tendency for all three models to simulate an outgoing longwave flux that is about 80 W m^{-2} too low, coinciding with the timing of the simulated cloud ice. The outgoing longwave flux simulated by the RCM is in much better agreement with the observations under cloud-free conditions, even though excessive water vapor is predicted (e.g., Julian day 301). This suggests the bias in the outgoing longwave flux is due to excessive high clouds rather

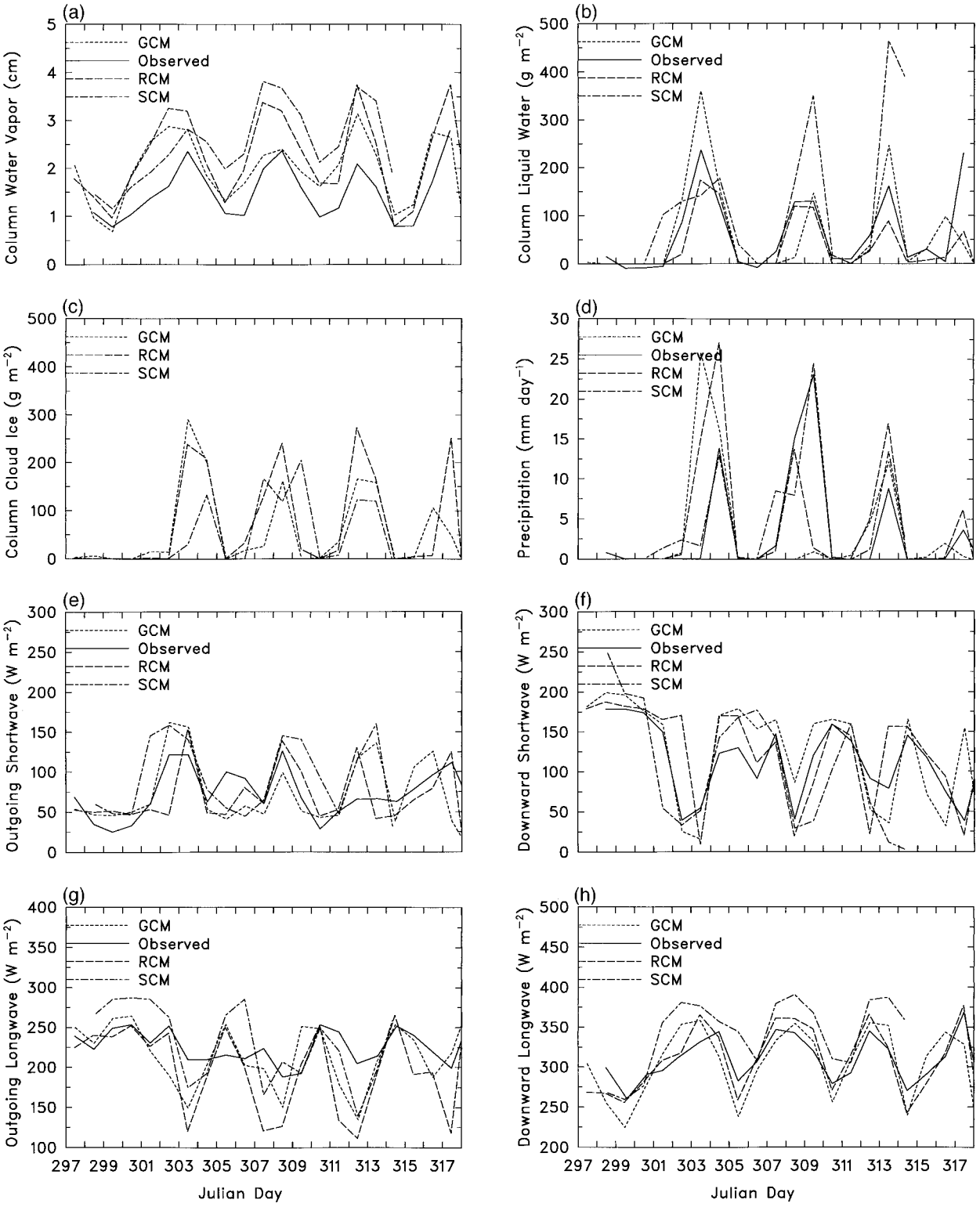

FIG. 9. (a) Daily mean column water vapor, (b) column cloud liquid water, (c) column cloud ice, (d) precipitation, (e) outgoing shortwave flux at the top of the atmosphere, (f) downward shortwave flux at the surface, (g) outgoing longwave flux at the top of the atmosphere,

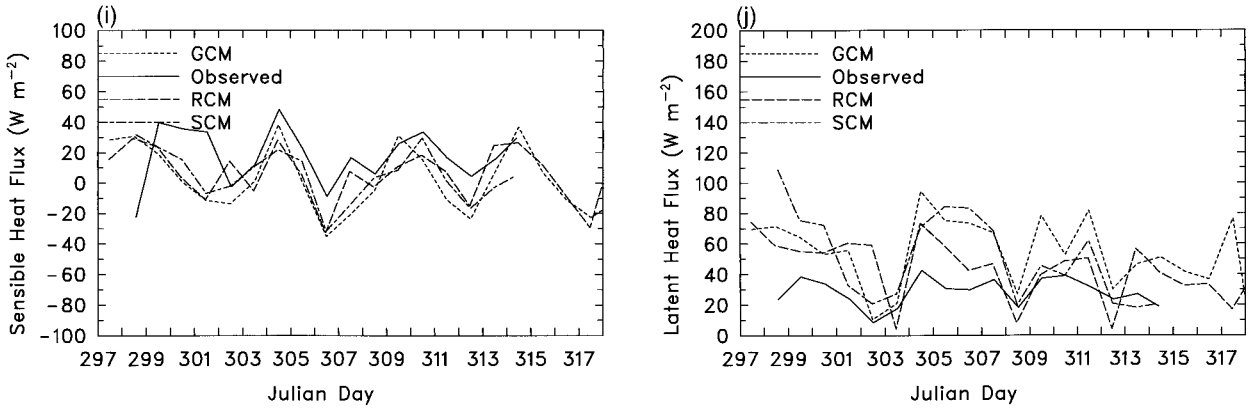

FIG. 9 (*Continued*) (h) downward longwave flux at the surface, and (i) surface fluxes of sensible and (j) latent heat observed at the SGP site and simulated by the GCM, the RCM, and by the SCM for the period 24 Oct–13 Nov 1994. The SCM simulation begins on Julian day 298 and ends on Julian day 314. Observations are not available for column cloud ice.

than excessive upper-tropospheric water vapor. The bias is common to all three models, suggesting that one model can be used as a testbed for correcting the bias in the other models.

The downward longwave flux at the surface (Fig. 9h) is controlled largely by water vapor. The RCM and GCM simulate the synoptic variability of the downward longwave flux quite well, with differences of typically less than 20 W m^{-2}. The downward longwave flux simulated by the SCM is usually about 20–50 W m^{-2} too high, but this bias is eliminated if humidity is nudged toward the analysis.

The turbulent surface fluxes of sensible and latent heat (Figs. 9i and 9j) simulated by the three models exhibit persistent biases, with the models simulating less sensible heat flux and more latent heat flux than observed. Although the gross features of the variability of the fluxes are simulated correctly, the simulated sensible heat flux is consistently about 20 W m^{-2} too weak and the simulated latent heat flux is consistently about 20 W m^{-2} too strong. Differences between models are usually less than 20 W m^{-2} for the latent heat flux and 10 W m^{-2} for the sensible heat flux. Thus, the surface flux biases in each model are indicative of the biases in the other models. These biases could be due to deficiencies in the model physics or in the initialization of soil moisture.

Much of the difference between the SCM simulation and the GCM and RCM simulations at the SGP site can be attributed to differences in the forcing. Figure 10 compares the column-integrated dynamical heating/moistening as simulated by the GCM and as analyzed by Zhang and Lin (1997) and used to drive the SCM. Although differences in the dynamic heating are less than 200 W m^{-2} on much of the time, differences exceed 1000 W m^{-2} at times. Differences in the dynamic moistening are less than 10 mm day^{-1} much of the time, but sometimes exceed 30 mm day^{-1}. Differences are particularly large on Julian days 303 and 304, when the dynamic heating (moistening) in the GCM is much lower (higher) than that in the wSCM. The greater moistening in the GCM simulation during this period does not lead to greater column water vapor because the heating is lower in the GCM simulation. Instead, the greater moistening produces more cloud liquid water, cloud ice, and precipitation in the GCM simulation, while the lower heating reduces the column water vapor.

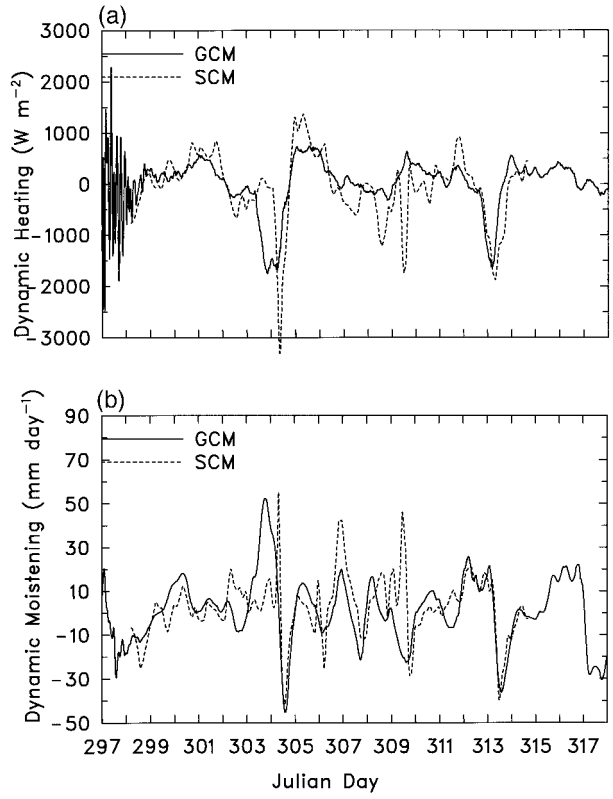

FIG. 10. (a) Column-integrated dynamical heating and (b) dynamic moistening at the SGP site as simulated by the GCM and as analyzed by Zhang and Lin (1997) and used to drive the SCM.

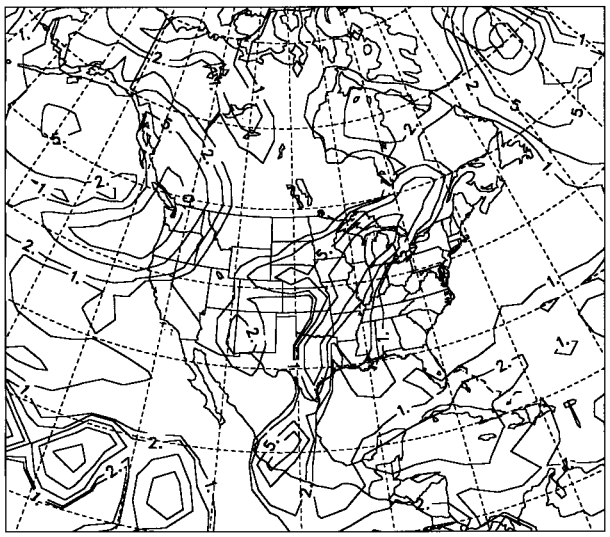

FIG. 11. Spatial distribution of the daily mean precipitation rate on 4 Nov 1994 as simulated by the the GCM. Contour levels are 1, 2, 5, 10, 20, and 50 mm day^{-1}.

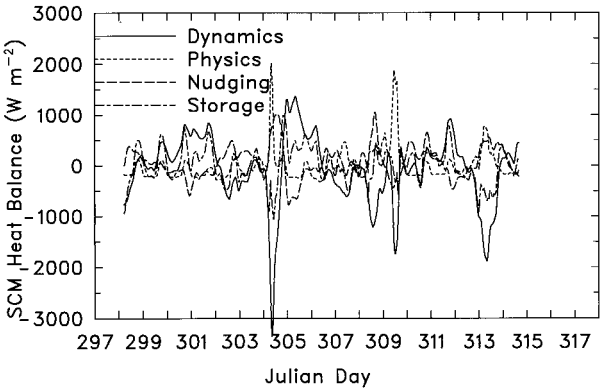

FIG. 12. Time series of the SCM column heat balance, including dynamical heating, physical heating, heating due to nudging, and heat storage.

One of the limitations of single-point evaluations of atmospheric circulation models is that when horizontal gradients are strong small errors in the simulated position of a cloud system can produce large local differences, even when the intensity and structure of the cloud system are simulated quite well. To illustrate this, Figs. 1 and 11 show the spatial distribution of precipitation on 4 November 1994 (Julian day 308) for the RCM and GCM simulations, respectively. Although according to Fig. 9d the precipitation rates at the T42 point closest to the SGP site in north-central Oklahoma differ by an order of magnitude, according to Fig. 10 the GCM simulates the peak precipitation rate for the Midwestern cloud system in fair agreement with the RCM, with peak rates of 16 and 26 mm day^{-1}. The cold front simulated by the GCM is more clearly defined, and the cloud system develops eastward of that simulated by the RCM. Agreement between the RCM and GCM simulations is much better at locations southeast of the SGP site.

How important is nudging in the SCM simulation? Figure 12 illustrates the four primary components of the SCM column heat budget, namely dynamics, physics, nudging, and storage. For some periods strong dynamical cooling is primarily balanced by physical heating, but for others the dynamical cooling is mainly balanced by nudging. Quite often nudging dominates physical heating, with nudging heating rates exceeding 1000 W m^{-2} on occasion. On those occasions the SCM simulates too little precipitation, which suggests that the strong nudging is correcting a physics deficiency rather than excessively strong dynamical cooling.

c. Sensitivity experiments

Although the differences between the SCM simulation and the simulations by the RCM and GCM are understandable, given the completely different analyses driving the simulations, the differences between the RCM and GCM simulations, even though they are not systematic, are disturbing because a primary goal of this study is to demonstrate the utility of the RCM as a testbed for GCM cloud parameterizations. To better understand the source(s) of these differences, we have performed two additional simulations designed to isolate potential sources of these differences.

The first such experiment addresses the difference in the domain of the RCM and GCM. Domain size is important because the water vapor and clouds are prescribed on the lateral boundaries of the RCM, whereas they are freely predicted in the GCM. Although the RCM domain cannot span the entire globe, it can be expanded from a 30 × 30 300-km grid to a 48 × 48 300-km grid so that it extends westward across the Pacific Ocean to Hawaii, southward to 20°S, and eastward to Spain. Figure 13 illustrates the influence of domain size on the simulated clouds. The column water vapor simulated by the larger domain RCM differs little from that simulated by the baseline domain RCM. The cloud liquid water is reduced by about 40% for the first cloud system, occurs 12 h earlier for the second, and is very similar to the baseline liquid water for the third and fourth cloud systems. Cloud ice is essentially unchanged for the first, third, and fourth cloud systems, but is about 50% greater than the baseline domain for the second cloud system. Precipitation is weaker in the first cloud system (consistent with the reduced cloud liquid water), stronger in the second cloud system (consistent with the enhance cloud ice), and unchanged in the third and fourth cloud systems. In none of the cloud systems is the RCM simulation with the larger domain closer to the GCM simulation than is the RCM simulation with the baseline domain. Although sensitivity to domain size is evident for some cloud systems, we cannot conclude that domain size is the primary explanation for differences between the RCM and GCM simulations.

Another source of differences between the RCM and

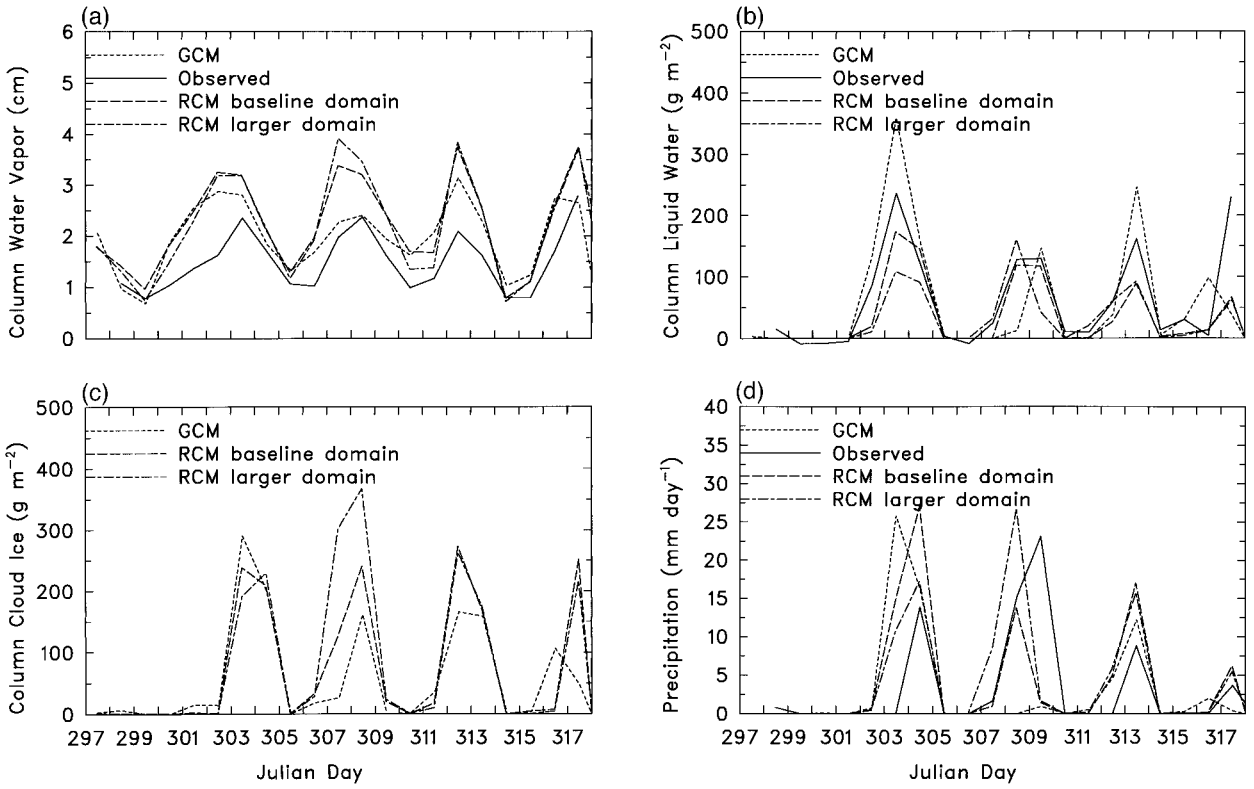

FIG. 13. (a) Daily mean column water vapor, (b) column cloud liquid water, (c) column cloud ice, and (d) precipitation observed at the SGP site and simulated by the GCM, by the RCM with baseline domain, and by the RCM with the larger domain for the period 24 Oct–13 Nov 1994. Observations of cloud ice are not available.

GCM simulations is the difference in the treatment of water transport. In the RCM, water is transported using the centered finite difference method for horizontal transport and using a harmonic mean finite difference method for vertical transport. In the GCM, water is transported using a semi-Lagrangian scheme (Williamson and Rasch 1994). We can evaluate the sensitivity to the treatment of water transport by either applying the GCM treatment to the RCM or by applying the RCM treatment to the GCM. We have chosen the latter option because the RCM treatment is simpler to apply. Figure 14 compares the RCM water vapor, cloud, and precipitation simulations with observations and with GCM simulations with semi-Lagrangian advection and with finite difference advection of water. The GCM simulation with finite difference advection is almost always closer to the GCM simulation with semi-Lagrangian advection than to the RCM simulation. The numerical treatment of water transport is therefore not an important source of differences between RCM and GCM cloud simulations.

If these two potential sources of differences between simulations are not important, then what are other potential sources? One might be the different horizontal grids in the RCM and GCM: although the average grid sizes are comparable, they cannot be made identical because the RCM uses a conformal map projection and the GCM uses a spherical grid. Another source might be the different vertical grids in the RCM and GCM: although the RCM levels have been chosen to match the GCM levels for a surface pressure of 1000 hPa, the RCM and GCM use different vertical coordinates (σ and η, respectively), which can yield different pressures when the surface pressure differs from 1000 hPa. A third source might be the different surface types used in the RCM and GCM simulations: although models use the BATS surface types, the types used in the RCM simulation were derived from the MM5 land use dataset, while those used in the GCM simulation were taken from the NCAR T42 BATS land use dataset.

5. Conclusions

In this study we have used three complementary test beds for evaluating cloud parameterizations for climate models: a global circulation model, a regional circulation model, and a single column model. Although all three models simulate the timing of cloud systems rather well, the intensity of the cloud systems differs substantially from model to model and from model to observation. Differences between the simulations and observations are to be expected because the analyses driving the models are imperfect and of course the models are imperfect. Differences between the SCM and the two

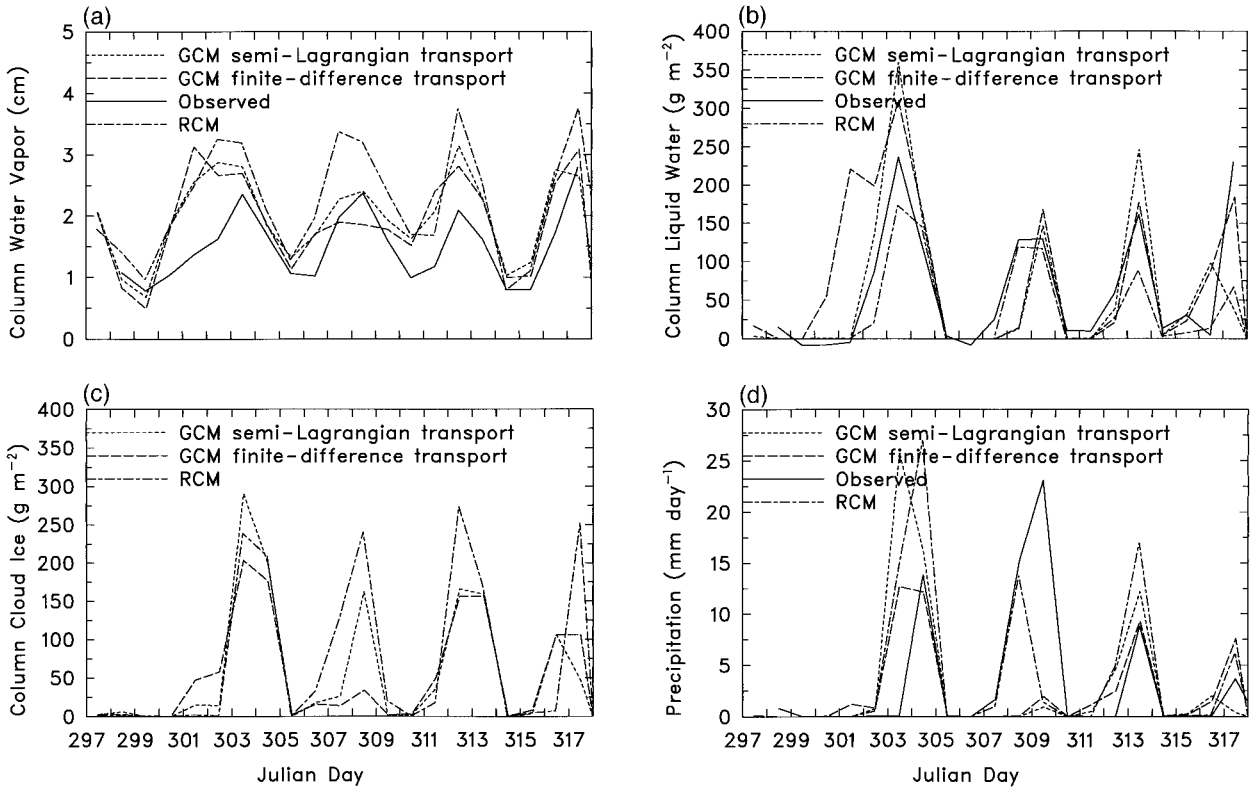

FIG. 14. Daily mean column water vapor (a), column cloud liquid water (b), column cloud ice (c), and precipitation (d) observed at the SGP site and simulated by the GCM with semi-Lagrangian advection, the GCM with finite difference advection, and by the RCM for the period 24 Oct–13 Nov 1994. Observations of cloud ice are not available.

circulation models are to be expected because the SCM is driven by an independent analysis. The differences between the RCM and GCM simulations are not systematic, instead varying from one cloud system to another, but are larger than might be expected given the common forcing used to drive the RCM and GCM.

We have conducted two sensitivity experiments designed to identify potential sources of the differences between the RCM and GCM simulations. An experiment in which the RCM treatment of moisture transport is applied to the GCM suggests that the differences in the treatment of moisture transport in the RCM and GCM are *not* important sources of differences in the cloud simulations. An experiment in which the RCM domain is increased yields results somewhat different from the simulation with a smaller domain, but no more similar to the GCM simulation.

Another potential explanation for differences between the RCM and GCM simulations is small differences in the spatial distribution of the fields when gradients are strong. Comparison of time series of each field has shown that small differences in the timing of cloud systems can introduce large differences in the instantaneous or even daily mean values of cloud and radiation fields, even if the maximum values are simulated accurately. Similarly, small differences in the position of cloud systems can produce large differences at a single point if the spatial gradients are large. Spatial averaging over larger areas than a single grid cell can reduce the sensitivity to errors in the position of cloud systems, but such averaging requires observations over a larger domain than the ARM CART site.

Other potential sources of differences between the RCM and GCM simulations are undetected differences in the treatment of model physics. Although the potential for such differences might be considered a significant disadvantage of using separate codes for regional and global simulations, it can also be considered an advantage because the search for errors to reconcile simulation differences can reveal bugs in each code. Indeed, in the course of our search for such differences we have identified bugs in both the RCM and GCM. Although a common code used as an SCM, an RCM, and a GCM (such as the Hadley Unified Model at the United Kingdom Hadley Center) offers some obvious advantages, bugs are more likely to remain undetected because they are common to all three modes of operation.

This study has relied heavily on a simple form of data assimilation, nudging, to constrain simulations and reduce the influence of dynamical instabilities and analysis errors on the simulated cloud and radiation fields. To provide a firmer foundation for this approach, we

have used a ''perfect'' model and ''perfect'' forcing to investigate the role of nudging in correcting errors in forcing and model physics. We have found that to some extent nudging can reduce the influence of analysis errors provided they are not too large, but that nudging can also hide errors in model physics. However, if the physics errors do not influence the nudged fields, then nudging of those fields will not hide those errors; only errors that influence the nudged fields are hidden by the nudging. Thus, if temperature and humidity are nudged, errors in nucleation, collision–coalescence, collection, and gravitational settling would not be hidden by nudging, while errors in radiative heating, condensation/vapor deposition, evaporation/sublimation, melting, cumulus convection, and transport (subgrid or large-scale) of heat and moisture would be hidden.

For most fields the differences between simulations and observations are not systematic and hence are probably due to errors in large-scale forcing or to the coarse resolution of the models. Three exceptions are the outgoing longwave radiation, the column water vapor, and the surface fluxes of sensible and latent heat. The outgoing longwave radiation is consistently too low in cloud systems simulated by all three models. This suggests the simulated clouds are too high, perhaps because of errors in the treatment of ice crystal size and gravitational settling, and points the way toward further experimentation to isolate and correct the problem.

The column water vapor is consistently too high in all three model simulations. This bias could be due to the absence of a subgrid treatment of stratiform clouds in the models, or to problems in the cumulus parameterization; the inconsistency between the observed convective precipitation and the simulated stratiform precipitation suggests that at least part of the problem is in the cumulus parameterization.

The surface sensible heat flux is consistently too low and the surface latent heat flux is consistently too high in all three model simulations. This bias could be due to deficiencies in the treatment of the fluxes, or more likely an initial soil moisture content that is too high. Simulations with the BATS land surface physics scheme replaced by the NCAR CCM2 treatment of surface physics (which prescribes soil moisture) yield consistently higher sensible heat flux and lower latent heat flux.

These three examples demonstrate the utility of using smaller (computationally faster) test beds (the SCM and RCM) to evaluate parameterizations for a GCM. For other variables (i.e., cloud water and precipitation), the systematic biases are smaller than differences between different model simulations for individual cloud systems. Although such differences are quite noticable for individual cloud systems, the differences vary from cloud system to cloud system. Simulations for longer or other periods are needed to identify systematic differences in these fields. Subsequent ARM IOPs have been analyzed and can be investigated using the three test beds described here. The additional surface stations and instruments at later periods can only improve the sampling and hence quality of the CART domain mean verification measurements.

Acknowledgments. Minghua Zhang and J. L. Lin of SUNY Stony Brook kindly provided their analysis of the SCM boundary conditions for the period. James Liljegren served as mentor for the MWR, developed the retrieval algorithms, and provided the data. Patrick Minnis of the NASA/Langley Research Center provided the earth radiation budget data. Douglas Cripe of Colorado State University provided the mean precipitation rate and surface flux data. The ARM Data Center provided the SIROS data. Dave Randall of Colorado State University suggested the use of advective nudging in the SCM. This research was supported by the Environmental Sciences Division of U.S. Department of Energy as part of the Atmospheric Radiation Measurement Program, which is part of the DOE Global Change Research Program. Pacific Northwest National Laboratory is operated for the DOE by Battelle Memorial Institute under Contract DE-AC06-76RLO 1830.

REFERENCES

Dickinson, R. E., A. Henderson-Sellers, and P. J. Kennedy, 1993: Biosphere–Atmosphere Transfer Scheme (BATS) version 1e as coupled to the NCAR Community Climate Model. National Center for Atmospheric Research Tech. Note NCAR/TN-387+STR, Boulder, CO, 72 pp.

GCSS Science Team, 1993: The GEWEX Cloud System Study. *Bull. Amer. Meteor. Soc.,* **74,** 387–400.

Ghan, S. J., and R. C. Easter, 1992: Computationally efficient approximations to stratiform cloud microphysics parameterization. *Mon. Wea. Rev.,* **120,** 1572–1582.

——, L. R. Leung, and Q. Hu, 1997: Application of cloud microphysics to NCAR CCM2. *J. Geophys. Res.,* **102,** 16 507–16 528.

Grell, G., J. Dudhia, and D. R. Stauffer, 1993: A description of the fifth-generation Penn State/NCAR Mesoscale Model (MM5). NCAR Tech. Note, NCAR/TN-397+IA, National Center for Atmospheric Research, Boulder, CO, 107 pp.

Hack, J. J., 1994: Parameterization of moist convection in the National Center for Atmospheric Research Community Climate Model (CCM2). *J. Geophys. Res.,* **99,** 5551–5568.

Holtslag, A. A. M., and B. A. Boville, 1993: Local versus nonlocal boundary-layer diffusion in a global climate model. *J. Climate,* **6,** 1825–1842.

Jeuken, A. B. M., P. C. Siegmund, L. C. Heijboer, J. Feichter, and L. Bengtsson, 1996: On the potential of assimilating meteorological analyses in a global climate model for the purpose of model validation. *J. Geophys. Res.,* **101,** 16 939–16 950.

Kiehl, J. T., J. J. Hack, and B. P. Briegleb, 1994: The simulated Earth radiation budget of the National Center for Atmospheric Research Community Climate Model CCM2 and comparisons with the Earth Radiation Budget Experiment (ERBE). *J. Geophys. Res.,* **99,** 20 815–20 827.

Lesht, B. M., and J. C. Liljegren, 1997: Comparison of precipitable water vapor measurements obtained by microwave radiometry and radiosondes at the Southern Great Plains Cloud and Radiation Testbed. *Proc. Sixth Atmospheric Radiation Measurement (ARM) Science Team Meeting,* San Antonio, TX, Department of Energy, 165–168. [NTIS CONF-9603149.]

Mace, G. G., and T. P. Ackerman, 1996: Assessment of error in synoptic scale diagnostics derived from wind profiler and radiosonde network data. *Mon. Wea. Rev.,* **124,** 1521–1534.

Minnis, P., W. L. Smith, D. P. Garber, J. K. Ayers, and D. R. Doelling, 1995: Cloud properties derived from *GOES-7* for spring 1994 ARM intensive observing period using version 1.0.0 of ARM satellite data analysis program. NASA Ref. Publ. 1366.

Moncrieff, M. W., S. K. Krueger, D. Gregory, J.-L. Redelsperger, and W.-K. Tao, 1997: GEWEX Cloud System Study (GCSS) working group 4: Precipitating convective systems. *Bull. Amer. Meteor. Soc.,* **78,** 831–845.

Petch, J. C., and J. Dudhia, 1998: The importance of horizontal advection of hydrometeors in a single column model. *J. Climate,* **11,** 2437–2452.

Randall, D. A., K.-M. Xu, R. J. C. Somerville, and S. Iacobellis, 1996: Single-column models and cloud ensemble models as links between observations and climate models. *J. Climate,* **9,** 1683–1697.

Stokes, G. M., and S. E. Schwartz, 1994: The Atmospheric Radiation Measurement (ARM) program: Programmatic background and design of the Cloud and Radiation Testbed. *Bull. Amer. Meteor. Soc.,* **75,** 1201–1221.

Westphal, D. L., and Coauthors, 1996: Initialization and validation of a simulation of cirrus using FIRE-II data. *J. Atmos. Sci.,* **53,** 3397–3429.

Williamson, D. L., and P. J. Rasch, 1994: Water vapor transport in the NCAR CCM2. *Tellus,* **46A,** 34–51.

Zhang, M. H., and J. L. Lin, 1997: Constrained variational analysis of sounding data based on column-integrated budgets of mass, heat, moisture and momentum: Approach and application to ARM measurements. *J. Atmos. Sci.,* **54,** 1503–1524.